Remote control of induced dopaminergic neurons in parkinsonian rats

Maria Teresa Dell'Anno,[1] Massimiliano Caiazzo,[1] Damiana Leo,[2] Elena Dvoretskova,[2] Lucian Medrihan,[2] Gaia Colasante,[1] Serena Giannelli,[1] Ilda Theka,[1] Giovanni Russo,[2] Liudmila Mus,[2,3] Gianni Pezzoli,[4] Raul R. Gainetdinov,[2,5,6] Fabio Benfenati,[2] Stefano Taverna,[2] Alexander Dityatev,[2,7,8] and Vania Broccoli[1]

[1]Stem Cell and Neurogenesis Unit, Division of Neuroscience, San Raffaele Scientific Institute, Milan, Italy. [2]Department of Neuroscience and Brain Technologies, Istituto Italiano di Tecnologia, Genoa, Italy. [3]Department of Psychopharmacology, Institute of Pharmacology, Pavlov Medical University, St. Petersburg, Russia. [4]Parkinson Institute, Istituti Clinici di Perfezionamento, Milan, Italy. [5]Skolkovo Institute of Science and Technology, Skolkovo, Moscow, Russia. [6]St. Petersburg State University, St. Petersburg, Russia. [7]German Center for Neurodegenerative Diseases (DZNE), Magdeburg, Germany. [8]Medical Faculty, Otto-von-Guericke University of Magdeburg (OVGU), Magdeburg, Germany.

Direct lineage reprogramming through genetic-based strategies enables the conversion of differentiated somatic cells into functional neurons and distinct neuronal subtypes. Induced dopaminergic (iDA) neurons can be generated by direct conversion of skin fibroblasts; however, their in vivo phenotypic and functional properties remain incompletely understood, leaving their impact on Parkinson's disease (PD) cell therapy and modeling uncertain. Here, we determined that iDA neurons retain a transgene-independent stable phenotype in culture and in animal models. Furthermore, transplanted iDA neurons functionally integrated into host neuronal tissue, exhibiting electrically excitable membranes, synaptic currents, dopamine release, and substantial reduction of motor symptoms in a PD animal model. Neuronal cell replacement approaches will benefit from a system that allows the activity of transplanted neurons to be controlled remotely and enables modulation depending on the physiological needs of the recipient; therefore, we adapted a DREADD (designer receptor exclusively activated by designer drug) technology for remote and real-time control of grafted iDA neuronal activity in living animals. Remote DREADD-dependent iDA neuron activation markedly enhanced the beneficial effects in transplanted PD animals. These data suggest that iDA neurons have therapeutic potential as a cell replacement approach for PD and highlight the applicability of pharmacogenetics for enhancing cellular signaling in reprogrammed cell–based approaches.

Introduction

The differentiated cell state has been traditionally considered irreversible and insensitive to epigenetic modifications. Nevertheless, in contrast with this classical view, accumulating evidence indicates that cell identity relies on a dynamic gene expression program that multiple physiological or pathological events might substantially alter (1–3). Pioneering work by Yamanaka and colleagues (4, 5) first illustrated how the genome of somatic cells is still highly responsive to the action of lineage-specific transcription factors (TFs) up to a full reestablishment of the pluripotency traits in adult cells. The induced pluripotent stem (iPS) cells can then be converted into different functional neuronal subtypes, offering unprecedented opportunities for cell-based therapies and disease modeling (6–11). Cell replacement therapy is particularly promising for diseases in which cell loss is relatively selective. A prototypical illness in this group is Parkinson's disease (PD), which is characterized by the loss of dopaminergic (DA) neurons that are located in the substantia nigra pars compacta and that specifically project to the striatum (12–14). The consequent loss of dopamine availability in striatal tissue is responsible for the motor impairments that severely affect PD patients. Embryonic stem cell/iPS cell–derived (ES/iPS-derived) DA neurons have been efficiently obtained from mouse and human cells and show efficacy when transplanted into PD animal models, alleviating motor symptoms (15–20). Nevertheless, the use of pluripotent-derived cells may lead to the generation of tumors whenever the differentiation procedure is not properly controlled (19–21).

An alternative method for the efficient generation of neuronal cells is direct lineage genetic reprogramming, which enables the direct conversion between 2 distinct somatic cell identities, bypassing the pluripotent stage. Vierbuchen et al. (22) first demonstrated the direct conversion of murine dermal fibroblasts into functional induced neuronal cells (iNs) through the forced expression of the factors ASCL1, BRN2, and MYT1L. The iNs can be produced from the conversion of human fibroblasts, a process enhanced by including additional TFs or microRNAs (23–26). During brain development, multiple genetic programs specifying DA neurons take place. Taking advantage of this knowledge (27–29), approaches for direct reprogramming have been developed to generate this particular neuronal subtype. We and others have presented minimal sets of neurodevelopmental TFs that are effective in converting mouse and human skin fibroblasts into functional induced DA (iDA) neurons (25, 30–32). Starting from mouse fibroblasts, the combined action of only *Ascl1*, *Nurr1*, and *Lmx1a* (ANL) efficiently generates iDA neurons. On the other hand, human fibroblasts have proved more resistant to conversion into iDA neurons, suggesting the need for additional factors and improved culture conditions (25, 33).

Induced neurons acquire a distinct neuronal morphology, express a wide repertoire of neuron-specific genes, and present sophisticated functional properties including an electrically excitable membrane, synaptic activity, and neurotransmitter synthesis

Conflict of interest: The authors have declared that no conflict of interest exists.
Citation for this article: *J Clin Invest.* 2014;124(7):3215–3229. doi:10.1172/JCI74664.

and release (26, 34–36). However, most of these studies have been conducted in vitro, and the phenotypic and functional stability of these cells after in vivo transplantation into the brain has not been directly assessed. In particular, what remains unknown is the degree to which the reprogrammed neurons functionally integrate into the host neuronal circuits and modulate their activity through this newly established connectivity. Obtaining such validation is crucial to verifying the reprogrammed neuronal state in a physiological setting and directly testing their functional correspondence with native brain neurons. Gaining full knowledge of their in vivo properties is necessary for devising appropriate approaches to maximize their therapeutic potential.

Here, we demonstrate that iDA neurons acquire a transgene-independent neuronal phenotype, maintaining all of their functional properties even after long-term engraftment in the brain tissue. This phenotypic stability is fully preserved, even when iDA neurons are transplanted into lesioned neural tissue. Furthermore, we combined neuronal reprogramming with the pharmacogenetic control of electrical properties and neurotransmitter release of the transplanted iDA neurons using DREADD (designer receptors exclusively activated by designer drug) technology (37, 38). DREADDs are mutated muscarinic receptors that are unresponsive to their endogenous ligand acetylcholine, while presenting a high potency for the pharmacologically inert molecule clozapine-N-oxide (CNO) (38, 39).

We showed that grafted iDA neurons significantly attenuated the motor impairments typical of PD rodents. Of importance, we could modulate the functionality remotely by peripheral CNO administration, thus potentiating the beneficial effects of these grafted iDA neurons. The combination of reprogramming and chemogenetic technologies proved to be useful for designing an innovative cell transplantation approach in a PD model, exerting efficient and noninvasive functional control of the grafted neuron's beneficial response.

Results

Transgene-independent functional stability of the reprogrammed neuronal state. We previously reported that fibroblast-reprogrammed iDA neurons maintain their neuronal phenotype after transgene silencing over time (30). However, it was not determined whether neuronal and synaptic functional activities were also irreversibly gained upon cell fate conversion. A similar concern remains for most of the other reprogrammed neuronal subtypes. Thus, we transduced mouse embryonic fibroblasts (MEFs) from TH-GFP transgenic animals with a mixture of doxycycline-inducible (dox-inducible) lentiviruses expressing the 3 reprogramming genes *Ascl1*, *Nurr1*, and *Lmx1a* (ANL, as noted above). After 4 days of dox induction, TH-GFP$^+$ cells were FACS sorted and replated on a culture of rat primary hippocampal neurons (Figure 1A). From day 8 onward, dox was removed from the culture medium, and TH-GFP$^+$ neurons were assessed for morphological and functional traits at 21 days in vitro (DIV). In this culture system, complete transgene silencing occurs 3 days after dox withdrawal (30). The 21-DIV iDA neurons exhibited a differentiated morphology (Figure 1B). Synaptotagmin 1$^+$ (SYT1$^+$) and HOMER1$^+$ puncta were easily detectable along TH-GFP$^+$ neurites, indicating the establishment and long-term maintenance of pre- and postsynaptic contacts, respectively (Figure 1, C and D). Of interest, the vesicular monoamine transporter protein 2 (VMAT2; NCBI: SLC18A2) was enriched in the synaptic contacts along the TH-GFP$^+$ fibers, confirming the monoaminergic identity of these neurons (Figure 1E).

To gain further evidence regarding the functionality of these synapses, we took advantage of the fluorescent false neurotransmitter FFN511, whose specific binding to the vesicular monoamine transporters enables optical imaging of presynaptic terminal activity (40). Importantly, we detected numerous FFN511$^+$ puncta along TH-GFP$^+$ fibers, indicating the presence of active presynaptic terminals competent in neurotransmitter uptake and release (Figure 1F). iDA neurons were then subjected to patch-clamp recordings to directly test their functional properties. These neurons could fire trains of action potentials (APs) when stimulated by current injection, and a large portion of them showed robust rhythmic discharges at a regular and sustained pace (Figure 1G). Furthermore, iDA neurons exhibited robust spontaneous synaptic activity that was blocked by the AMPA receptor antagonist NBQX (Figure 1H). These results demonstrate that iDA neurons irreversibly adopt the reprogrammed neuronal state by 8 days of transgene expression and show stable functional properties of spontaneous firing of APs and robust synaptic activity.

We then tested the gene expression levels of cardinal molecules of DA neuronal fate and biochemical synthesis after transgene removal on a pure population of FACS-sorted iDA cells (Supplemental Figure 1; supplemental material available online with this article; doi:10.1172/JCI74664DS1). Despite the fact that iDA neurons have low levels of *Pitx3* and *Foxa2* transcripts, they showed elevated expression levels of *Foxa1*, *En1*, and *En2*, comparable to those observed in freshly isolated TH-GFP$^+$ E13.5 primary DA neurons (Supplemental Figure 1). Moreover, *Th* and *Vmat2* gene expression was equivalent in both neuronal cell types, while *Ddc* and *Dat* (NCBI: SLC6A3) expression levels were not as high in reprogrammed cells compared with those in primary DA neurons (Supplemental Figure 1). Altogether, these data suggest that iDA neurons can stably acquire the expression of cardinal genes of DA midbrain regional specification, although 2 important molecular codes, *Pitx3* and *Foxa2*, remained at low levels, at least in in vitro cultures. Of note, the expression of critical components of dopamine synthesis, release, and uptake was strongly induced and maintained after DA neuronal conversion.

Stability of iDA neuronal identity after transplantation in vivo. Despite the notion that direct neuronal reprogramming can represent a valuable method for generating transplantable neurons, the properties of induced neurons after in vivo transplantation have been only partially analyzed thus far. Accordingly, we aimed to determine the transgene-independent stability of the reprogrammed neuronal phenotype after in vivo transplantation upon transgene withdrawal. To assess whether iDA neurons regress to the cell type of origin (fibroblasts) after in vivo transplantation and in the absence of dox, we devised a double-reporter cell-tracing strategy that consisted of labeling reprogrammed TH-GFP$^+$ neurons with a constitutively expressed tdTomato reporter. This system enables tracing of the TH-GFP$^+$ neurons independently of their reprogrammed neuronal fate and can identify them even in situations in which they would revert to a fibroblast phenotype. Thus, the DIV 4–induced TH-GFP$^+$ cells were separated by the remaining nonreprogrammed fibroblasts by FACS sorting and then replated and transduced with a lentivirus expressing the tdTomato reporter under the constitutive ubiquitin promoter.

In these conditions, 90% of TH-GFP$^+$ cells expressed tdTomato before they were engrafted into the striatum of 3-week-old immunodeficient *Rag2*$^{-/-}$ *Il2rg*^{tmWjl}–null mice. We then divided the trans-

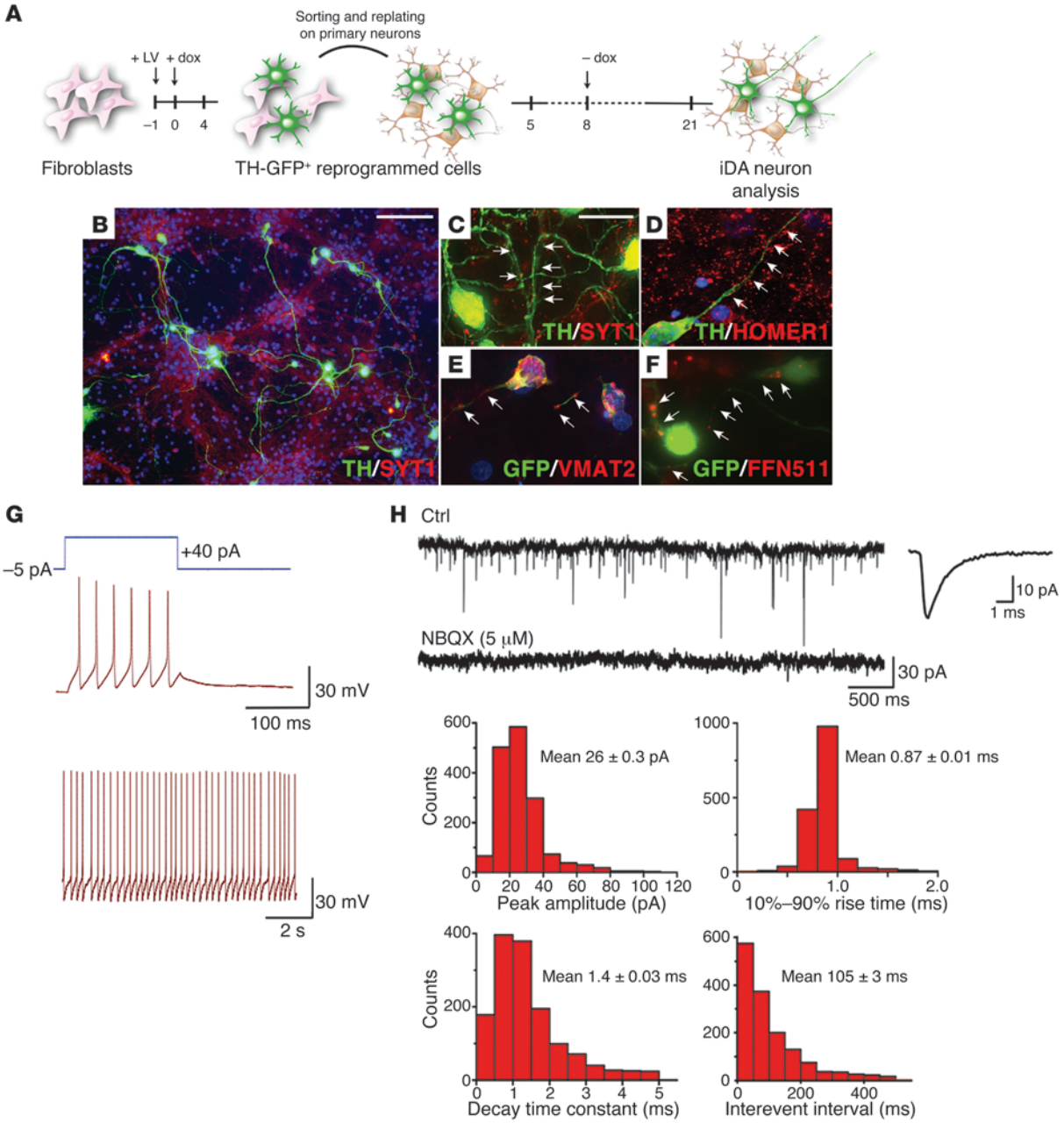

Figure 1

Morphological and functional stability of the reprogrammed state of iDA neurons in vitro. (**A**) Scheme showing the experimental procedures for coculturing iDA cells and primary hippocampal neurons in the absence of dox. iDA neurons were FACS sorted on day 4 and directly plated onto primary cell cultures. From day 8, dox was removed, and cells were left in culture until day 21, when morphological and functional analyses were performed. LV, lentivirus. (**B**–**D**) Immunocytochemical analysis of iDA neurons in vitro after dox withdrawal. iDA neurons exhibited a differentiated morphology and long projections, with SYT1 and HOMER1$^+$ puncta located along neurites. (**E** and **F**) Immunodetection of VMAT2 and its functional assessment on iDA neurons through FFN511. (**G**) Current-induced and spontaneous trains of APs recorded in iDA neurons at 21 DIV. (**H**) Spontaneous glutamatergic EPSCs at 21 DIV in iDA neurons recorded in voltage-clamp mode (V_h: –60 mV; top trace). After application of the AMPA receptor antagonist NBQX (5 μM), the EPSCs were completely blocked (bottom trace). Inset shows an averaged EPSC in an expanded time scale (n = 20 spontaneous events). Histograms show the distributions of the basic EPSC parameters. Scale bars: 50 μm (**B**), 10 μm (**C**–**F**). Data shown in **B**–**H** are representative of 3 independent experiments performed on 6 samples.

planted mice into 4 experimental groups that received dox, respectively, for 0, 6, or 12 days or for 5 weeks, at which point all animals were sacrificed for analysis (Figure 2A). Immunohistochemical analysis of the transplanted tissue in the first experimental animal group that did not receive dox showed a subset of tdTomato$^+$-transplanted cells that lost both neuronal morphology and TH-GFP expression (Figure 2, B–D; arrows in D). Of note, triple immunostaining revealed that tdTomato$^+$TH-GFP$^-$ cells

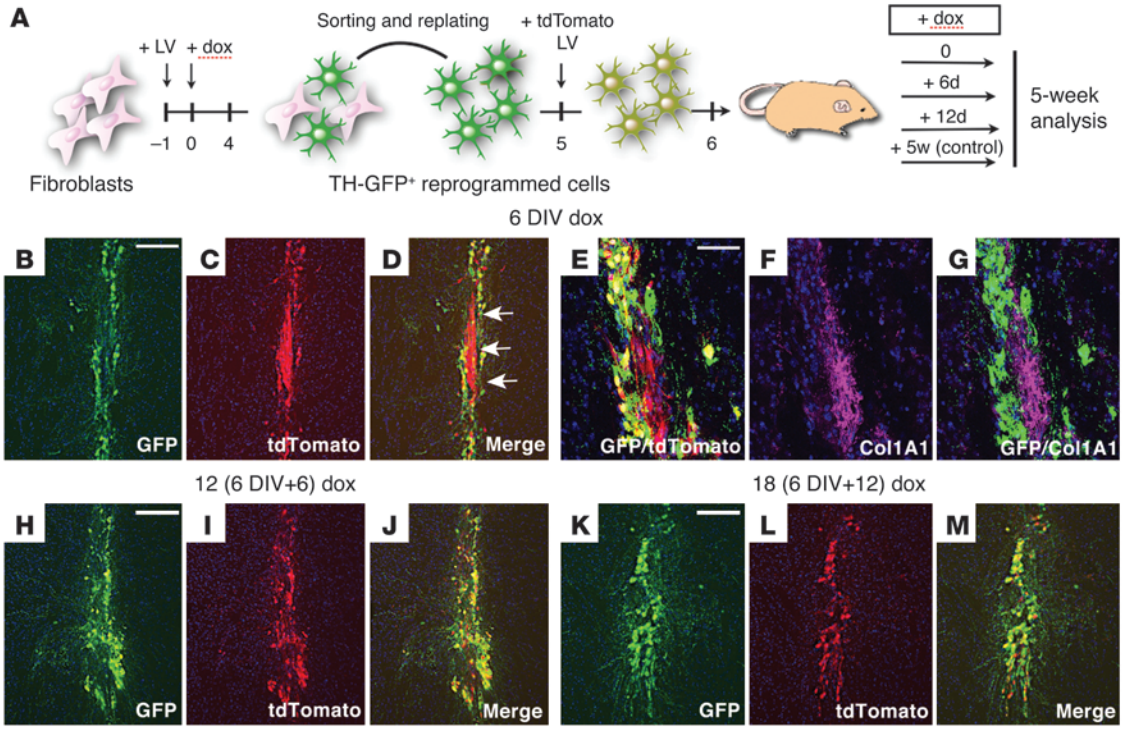

Figure 2

Analysis of the reprogrammed neuronal phenotype of iDA neurons in vivo at different times of dox administration. (**A**) Schematic representation of lentiviral infection of iDA neurons before transplantation. Reprogrammed cells were FACS sorted on day 4 and replated at high density for tdTomato lentiviral infection on day 5. iDA neurons were left in culture for 24 hours and then grafted into the striatum of *Rag2*$^{-/-}$ *Ilrg*^{tmWjl}–null mice. (**B**–**D**) Immunohistochemical assay of grafted iDA neurons after 6 days of dox exposure in vitro. Immunostaining reveals the presence of tdTomato^{+}TH-GFP^{-} cells with fibroblast-like morphology. (**E**–**G**) tdTomato^{+} cells were also positively stained for collagen I, confirming their regression to fibroblasts. (**H**–**J**) Immunohistochemistry of grafted iDA neurons after 6 DIV plus 6 days in vivo of dox administration revealed the coexpression of both tdTomato and GFP reporters. A comparable result was obtained by extending dox administration in vivo from 6 to 12 days (**K**–**M**). Scale bars: 100 μm (**B**–**D**), 30 μm (**E**–**G**), 100 μm (**H**–**M**). **B**–**M** are representative images of 3 independent experiments performed on 3 mice per group.

expressed collagen I, indicating that this subset of iDA neurons reverted to a fibroblast-like phenotype after grafting into the brain parenchyma (Figure 2, E–G).

We then analyzed the transplanted site in the animal groups that received dox for extended time periods (6 days, 12 days, or 5 weeks). In all cases, double staining for GFP and tdTomato revealed complete coexpression of both reporters in all transplanted cells, showing a well-matured neuronal morphology (Figure 2, H–M, and Supplemental Figure 2). These data demonstrate that after sufficient induction of the transgenes, the iDA neuronal phenotype becomes stable even upon transplantation into the host brain parenchyma. Of importance, 12 days of dox treatment (6 DIV followed by 6 days in vivo) were sufficient to achieve a stable neuronal reprogrammed state, which persisted for at least 5 weeks after brain transplantation.

Functional integration of the transplanted iDA neurons in the host neuronal circuits. We then asked whether the neuronal reprogrammed state could stably inherit the functional properties that define a neuronal identity in an in vivo setting. Initially, we asked whether transplanted iDA neurons establish enduring synaptic contacts with the host neurons. We thus loaded iDA neurons with the synaptic tracer wheat germ agglutinin (WGA) and assessed its trans-synaptic uptake in the surrounding neurons. In particular, DIV 4–induced TH-GFP^{+} cells were FACS sorted, replated, and transduced with a lentivirus constitutively expressing the WGA (Figure 3A). Subsequently, TH-GFP-WGA double-positive cells were either cocultured with primary mouse E14.5 ventral telencephalic neurons or injected into the striatum of 3-week-old immunodeficient *Rag2*$^{-/-}$ *Ilrg*^{tmWjl}–null mice (Figure 3G; n = 4). For in vitro experiments, dox was withdrawn on day 8, while it was administered for an additional 6 days after transplantation into animals (Figure 3A). Of interest, the trans-synaptic transfer of WGA was confirmed under both conditions by detection of numerous WGA^{+}TH-GFP^{-} healthy cells that accumulated the tracer in the cytoplasm surrounding the nucleus (Figure 3, B–F; arrows in C, D, H, and I). Moreover, the in vitro experiments showed that WGA^{+}TH-GFP^{-} cells colocalized with the GABAergic marker GAD, proving that iDA neurons are able to make synaptic contacts with GABAergic neurons (Figure 3, E and F). Accordingly, the in vivo experiments proved that WGA^{+}TH-GFP^{-} cells colocalize with the pan-neuronal marker NeuN, thus confirming that, also in the host brain, iDA neurons establish functional synapses with resident neurons (Figure 3, J and K).

We then sought to determine the intrinsic electrophysiological properties of iDA neurons 5 weeks after transplantation into the striatum of immunodeficient *Rag2*$^{-/-}$ *Ilrg*^{tmWjl}–null mice. Patch-clamp recordings were performed in a whole-cell configuration on TH-GFP^{+} iDA neurons visually identifiable on brain slices (Figure 4,

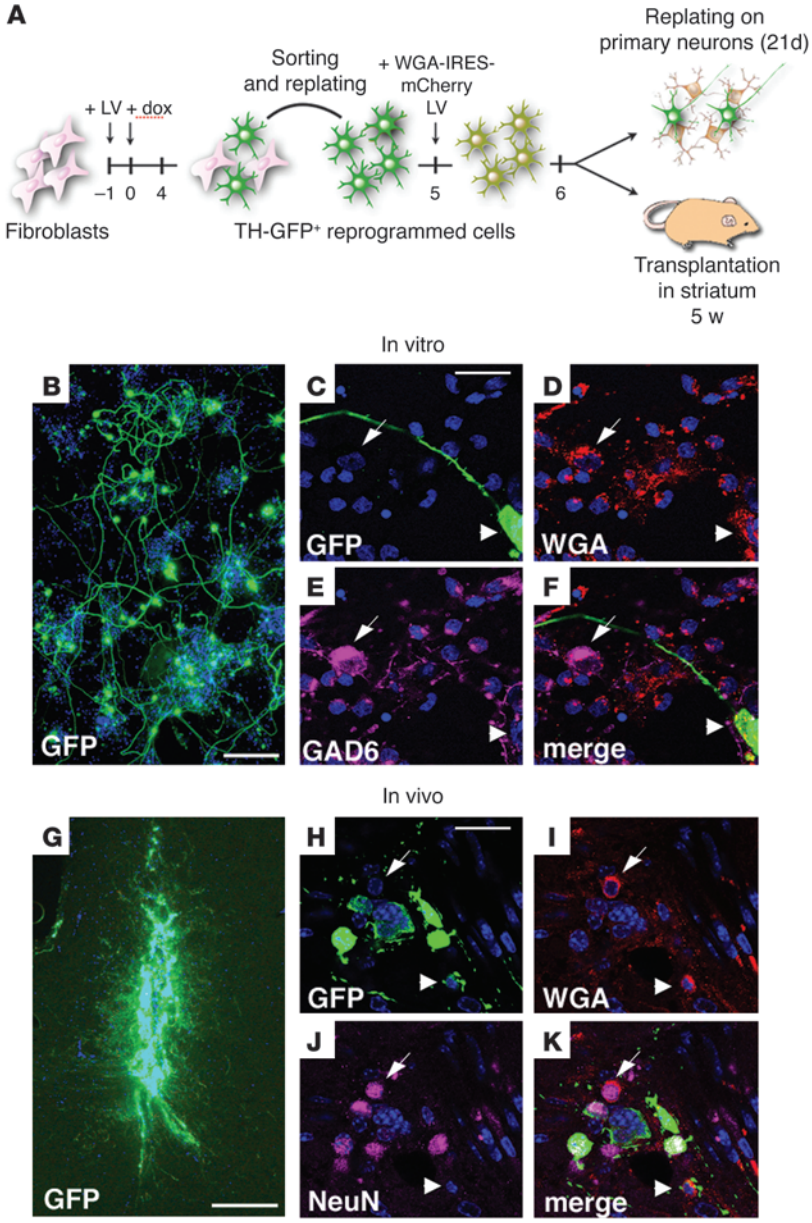

Figure 3
WGA synaptic tracing of iDA neurons in vitro and in vivo. (**A**) iDA neurons were infected with WGA-IRES-mCherry lentivirus 1 day after sorting and then replated on mouse MGE primary cell culture for in vitro analysis. (**B**) iDA neurons showed dense arborization after 21 DIV and were able to establish functional synaptic contacts with mouse primary cells. (**C**–**F**) Staining for WGA clearly revealed WGA^+GFP^- cells, demonstrating that WGA from infected iDA neurons was uptaken from surrounding GAD^+ neural cells through functional synapses. (**G**) iDA neurons expressing WGA were also transplanted into the striatum of immunodepressed mice (n = 4), and animals were kept alive for 5 weeks. (**H**–**K**) Immunohistochemistry shows WGA^+GFP^- cells in the host tissue. These cells were also positive for NeuN, as shown in triple immunostaining, thus proving the ability of iDA neurons to establish synaptic connections with neighboring neurons after grafting. Scale bars: 60 μm (**B**), 20 μm (**C**–**F**), 200 μm (**G**), 20 μm (**H**–**K**). **B**–**K** are representative images from 3 independent experiments performed on 4 mice per group.

A and B). The identity of the recorded neurons was then confirmed by filling the patched neurons with biocytin, followed by retrospective immunolabeling for GFP or TH, as shown in the representative pictures in Figure 4, C–E. In voltage-clamp configuration, iDA neurons showed robust Na^+ and K^+ currents in response to 10-mV step changes in membrane potential (V_m) (Figure 4F). In current-clamp mode, iDA neurons displayed a physiological membrane potential (–50 mV; n = 6) and responded to step current injections (50–150 pA, 500 ms) by firing APs once the voltage threshold was reached (Figure 4G). Under these conditions, a single AP or a burst was followed by pronounced firing inactivation; however, slow injection of a suprathreshold current induced sustained AP firing (Figure 4H).

Finally, we tested whether grafted iDA neurons were synaptically integrated into the host striatal network. Of interest, upon loading of the fluorescent false neurotransmitter FFN511 onto transplanted brain slices, we detected numerous $FFN511^+$ puncta along $TH\text{-}GFP^+$ fibers, indicating the presence of functional presynaptic terminals competent in neurotransmitter uptake and release (Figure 4I). Finally, we recorded spontaneous excitatory and inhibitory postsynaptic currents from $TH\text{-}GFP^+$ iDA neurons that were blocked by the AMPA- and GABA.receptor–specific antagonists NBQX (5 μM) and gabazine (10 μM), respectively (Figure 4J). These data are unprecedented, providing the first evidence to our knowledge that neurons obtained through direct cell reprogramming can establish and receive functional synaptic contacts and therefore integrate into the host circuitry. Overall, these results suggest that iDA neurons transplanted into the striatum of healthy mice retain the phenotype of electrically excitable cells and maintain functional synaptic connections with neighboring neurons.

Long-term DA phenotypic stability of iDA neurons after transplantation into 6-hydroxydopamine–lesioned rats. Neuronal reprogramming might provide a new opportunity for the straightforward genera-

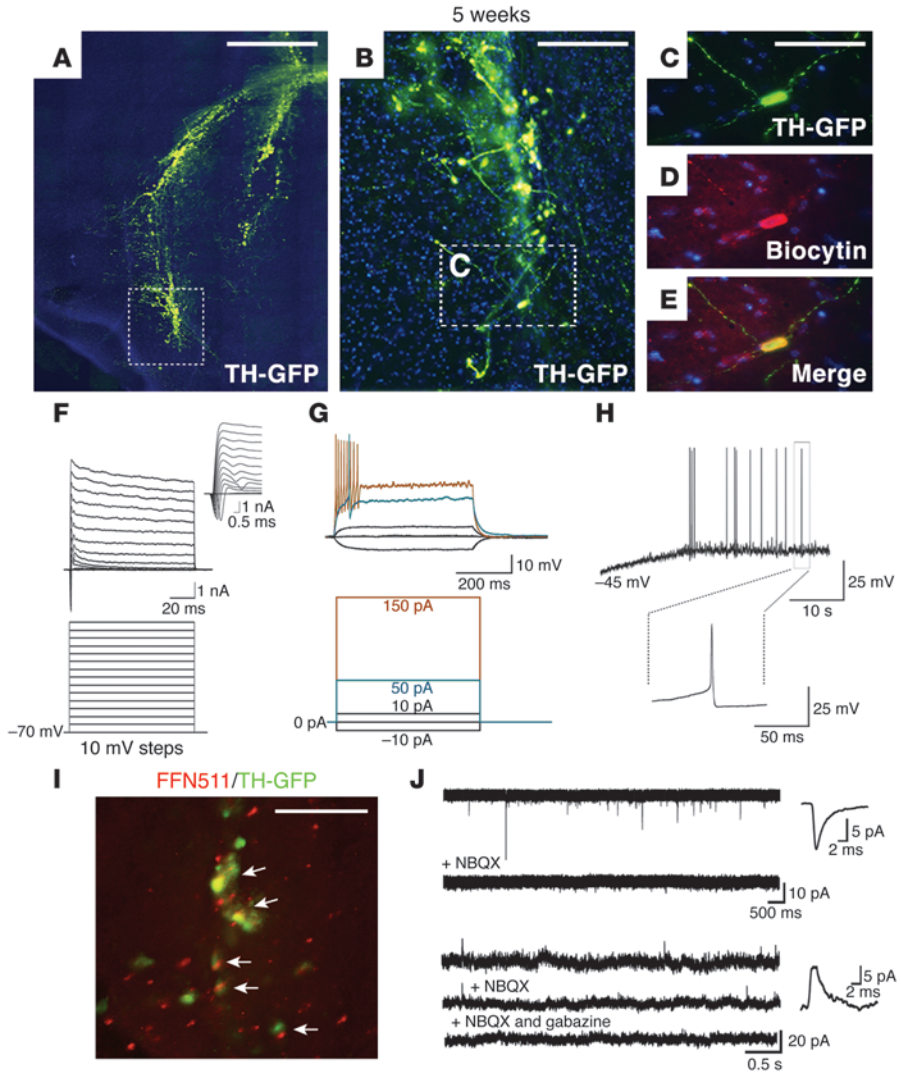

Figure 4
Functional integration of transplanted iDA neurons. (**A** and **B**) Immunohistochemistry of iDA neurons grafted into immunodepressed mice for electrophysiological recordings. (**C**–**E**) High magnification of a biocytin-filled reprogrammed neuron immunostained for GFP. (**F**) Voltage-dependent Na^+ (negative-going) and K^+ (positive-going) currents in response to 10-mV steps (starting from a V_h of –70 mV) in voltage-clamp mode. Inset shows a magnified view of the first portion of the traces. (**G**) Voltage responses of an iDA neuron to hyperpolarizing and depolarizing current steps in current-clamp mode. (**H**) Continuous AP firing was induced by a slow suprathreshold current ramp (~4 pA/second). (**I**) Assessment of FFN511$^+$ synaptic terminals on transplanted TH-GFP$^+$ iDA neuronal fibers in brain slices. (**J**) Upper panel: sEPSCs recorded at a V_h of –70 mV were blocked by the extracellular application of 5 μM NBQX. Lower panel: sIPSCs recorded at a V_h of 0 mV were blocked by the extracellular application of 10 μM gabazine. Insets show averaged EPSCs and IPSCs, respectively, in an expanded time scale. Scale bars: 600 μm (**A**), 150 μm (**B**), 50 μm (**C**–**E**), 100 μm (**I**). **A**–**J** are representative images of 3 independent experiments performed on 3 mice and 6 cells (**F**–**J**).

tion of neurons suitable for brain repair. Thus, we decided to challenge iDA neurons upon engrafting them into a lesioned brain parenchyma. An extensive unilateral lesion of the nigrostriatal pathway can be reliably achieved by a single stereotaxic injection of 6-hydroxydopamine (6-OHDA) into the striatum. The extent of the lesion can be verified postmortem by immunohistochemistry for TH, as illustrated in Figure 5A. For behavioral and functional assays, the damage can also be assessed through subcutaneous injection of the dopamine agonist apomorphine. In fact, apomorphine predominantly activates the denervated striatum on the lesioned side, thus triggering a quantifiable rotational behavior. In the present study, only animals performing more than 6 rotations per minute were included in the behavioral analysis. For the transplantation procedure, DIV 4–induced TH-GFP$^+$ cells were FACS sorted and replated in high-density cultures before being grafted into the 6-OHDA–lesioned striatum (Figure 5A). A total of 5×10^5 TH-GFP$^+$ cells were grafted into 2 independent sites of the lesioned striatum, and dox treatment was discontinued 6 days after transplantation for a total of 12 days of dox-dependent expression of the reprogramming genes. To verify the long-term survival and behavior of transplanted iDA neurons, the treated rats were kept for 8 weeks before morphometric and functional inspection. DAB immunohistochemistry on brain slices of engrafted animals highlighted a large cluster of GFP$^+$ cells in the transplantation site that at higher magnification exhibited a mature neuronal morphology (Figure 5, B and C). Of note, we observed an appreciable fiber outgrowth extending long distances into the denervated host striatal tissue and emerging from the grafted GFP$^+$ iDA neurons (Figure 5D). Double immunolabeling showed that the majority of grafted TH-GFP$^+$ iDA neurons expressed TH, VMAT2, and AADC, thus confirming their phenotype (Figure 5, E–K, and Supplemental Figure 3). Moreover, a large number of iDA neurons were immunostained for DAT, corroborating their specific DA identity and terminal maturation (Figure 5L and Supplemental Figure 2). These data demonstrate that iDA neurons survive and entirely preserve their reprogrammed neuronal phenotype for a long time after engrafting into the lesioned brain tissue, independently of transgene expression.

To gain evidence for the functionality of the grafted iDA neurons, we tested their ability to produce and release dopamine. Fast-scan cyclic voltammetry (FSCV) measurements on striatal slices containing the graft revealed a significant increase in evoked

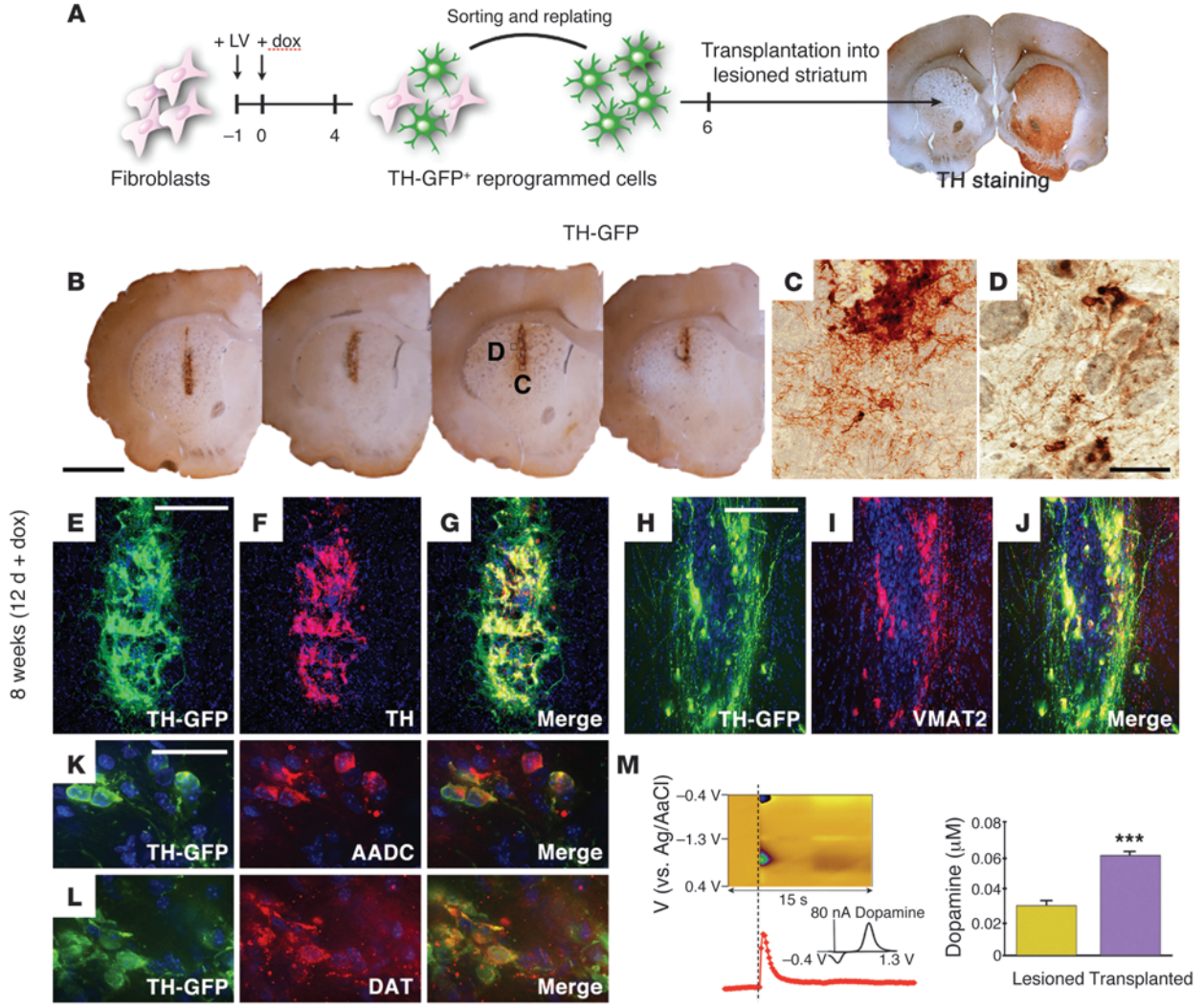

Figure 5

Transplantation of iDA neurons in 6-OHDA–lesioned rats. (**A**) Before transplantation in parkinsonian rats, iDA neurons were FACS sorted and separated from nonreprogrammed fibroblasts. Animals were kept alive for 8 weeks and then sacrificed for tissue processing. (**B**–**D**) Immunohistochemistry shows a consistent cluster of GFP+ cells with an extended net of neurites innervating the host striatum. (**E**–**L**) Transplanted cells retained their phenotype in vivo, as shown by the immunodetection of the dopamine markers TH, VMAT2, AADC, and DAT. (**M**) FSCV of grafted parkinsonian rats revealed a significant increase of dopamine in iDA neuron–transplanted versus control-lesioned striatum. Data represent the means ± SEM ($n = 3$). ***$P < 0.001$, Student's t test. Scale bars: 600 μm (**B**), 30 μm (**C** and **D**), 200 μm (**E**–**G**), 100 μm (**H**–**J**), 30 μm (**K** and **L**). **B**–**M** are representative images from 3 independent experiments performed on 3 rats per group.

dopamine release compared with levels detected in the denervated striatal tissues (Figure 5M). Taken together, these observations indicate that the neuronal reprogrammed state is maintained even after a long exposure to harsh pathological conditions that severely affect and compromise local homeostasis.

iDA neurons are resistant to tumorigenic growth in vivo. To assess tumorigenic potential, DIV 4–induced TH-GFP+ cells were FACS sorted, replated, and transplanted the following day into 3-week-old immunodeficient *Rag2*$^{-/-}$ *Ilrg*^{tmWjl}–null mice, a strain that efficiently supports xenograft survival with particular sensitivity to rare tumorigenic cells (41). At 5 and 12 weeks after transplantation of about 5×10^5 iDA neurons ($n = 10$), we tested the integration and proliferation of the grafted cells. At both stages analyzed, we observed a large graft of TH-GFP+ transplanted cells with an elaborated neuronal morphology and long processes extending into the host neural tissue (Supplemental Figure 4, A and B). Despite the large number of grafted cells, we could not identify tissue overgrowth at the transplantation site (Supplemental Figure 4, A and B). Accordingly, none of the transplanted iDA neurons were positive for Ki67 or nestin, 2 markers associated with cell division and the neural progenitor state, respectively (Supplemental Figure 4E; data not shown). By contrast, Ki67+ cells were easily detectable in the striatal subventricular zone of the same sections, where neurogenic processes were ongoing, confirming the quality of the immunolabeling assays. Taken together, these data demonstrate that reprogrammed DA neurons can survive for a long time in the injection site without showing any sign of uncontrolled proliferative behavior or reverting to a progenitor neuronal state.

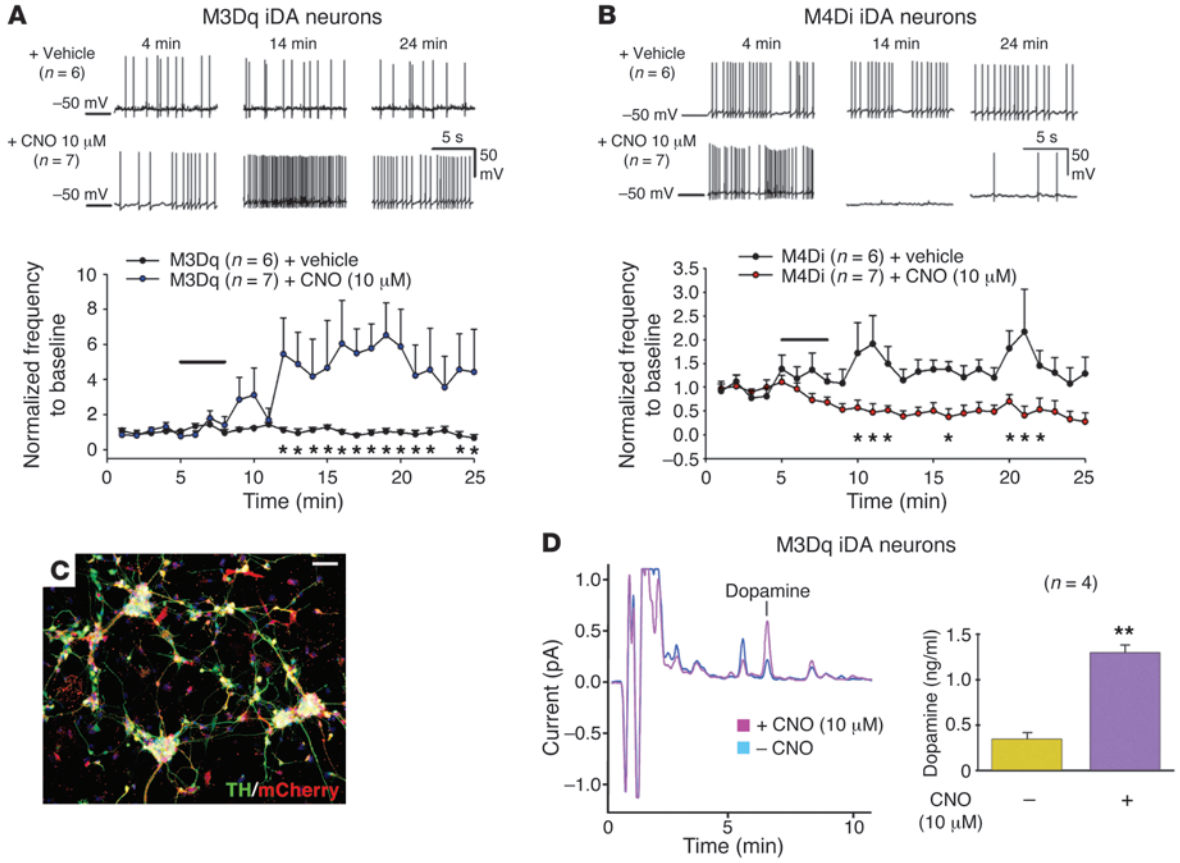

Figure 6

Functional assessment of DREADD activity in iDA neurons in vitro. (**A**) Upper panels: Whole-cell patch clamp recordings of M3Dq iDA neurons (**A**) and M4Di iDA neurons (**B**) at various times after vehicle and CNO (10 μM) application. Lower panels: time course of the normalized firing rate (mean ± SEM) as a function of time after vehicle (black circles) or CNO (red and blue circles) application (horizontal line). *$P < 0.05$, 2-way ANOVA followed by post-hoc Bonferroni-Dunn tests. (**C**) Immunocytochemistry of M3Dq iDA neurons for mCherry and TH. Scale bar: 50 μm. (**D**) Representative HPLC chromatogram in a sample of M3Dq iDA neurons with and without CNO (10 μM) application. Bars show the estimated concentration of dopamine in control and CNO-treated cells. **$P < 0.005$ by Student's *t* test. Data shown in **A**–**C** are representative of 3 independent experiments performed on at least 6 cells.

Generation and functional assessment of CNO-responsive M3Dq iDA neurons. As described above, transplanted iDA neurons demonstrated long-term survival, activity, and functional integration into the host neural parenchyma. Next, we asked whether pharmacological modulation of the activity of transplanted iDA neurons is sufficient to influence the overall functionality of the host neuronal network, thus eliciting detectable behavioral responses in the grafted animals. To this end, we decided to combine the iDA neuronal reprogramming with DREADD technology. Currently, 2 distinct forms of DREADDs have been designed to elicit opposite effects on neuronal activity. The DREADD M4Di, coupled with the inhibitory Gi protein, activates the G protein inward-rectifying potassium channels in response to CNO and triggers membrane hyperpolarization and inhibition of AP firing (38). On the other hand, the DREADD M3Dq, associated with the stimulatory Gq protein, elicits robust Ca^{2+} mobilization and membrane depolarization, thus increasing the firing rate (37). DREADD receptor activity has been investigated in both non-neuronal and neuronal cells (37, 38, 42). However, it is unknown whether DA neuronal activity is responsive to DREADD-induced intracellular signaling. To clarify this issue, we established primary neuronal cultures from E13.5 ventral midbrain tissue from TH-GFP transgenic mice. DIV 4 cultures were then transduced with lentiviruses expressing either the M3Dq or the M4Di DREADD together with the mCherry reporter (Supplemental Figure 5A). When neuronal maturation was achieved (14 DIV), we patch clamped double GFP-mCherry$^+$ neurons to record their spontaneous neuronal activity and its dependence on CNO stimulation. M3Dq-expressing DA neurons responded to CNO treatment with a short delay and for several minutes by strongly increasing their AP firing rate (Supplemental Figure 5B). In contrast, CNO administration to M4Di-expressing DA neurons caused a sudden arrest in AP firing that also persisted for several minutes (Supplemental Figure 5C).

We then performed similar recordings using iDA neurons. In particular, TH-GFP fibroblasts, reprogrammed with the ANL factor cocktail, were transduced with lentiviruses expressing either M3Dq or M4Di together with the mCherry reporter. Most of the reprogrammed iDA neurons showed bright mCherry expression, enabling straightforward visualization of the double-positive neurons (Figure 6C). At 14 DIV, patch-clamp recordings were performed on iDA neurons to test CNO effects on their activity. M3Dq-expressing iDA neurons responded to CNO treatment by

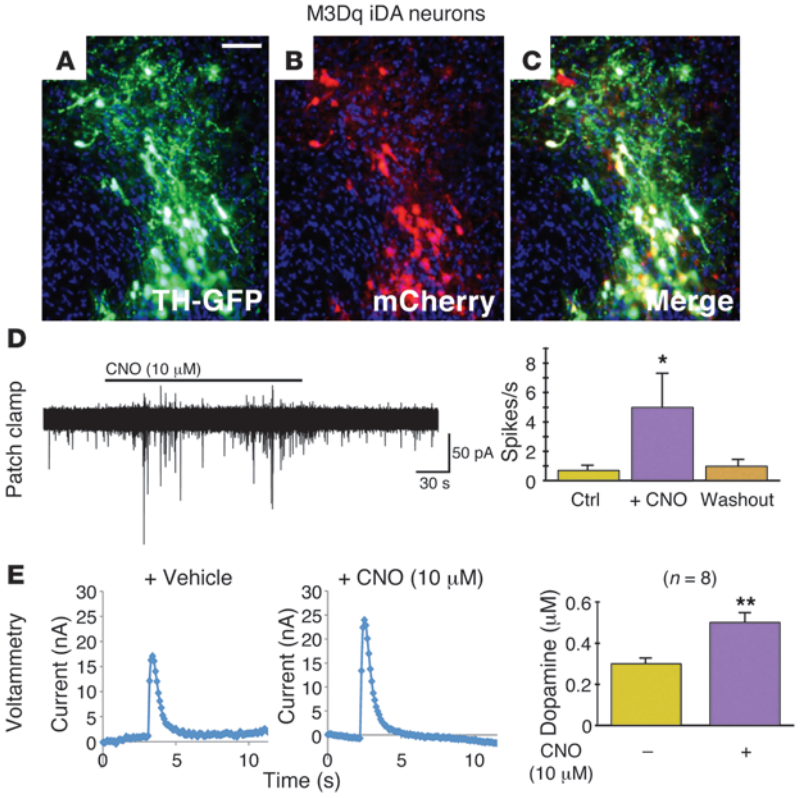

Figure 7
Functional assessment of DREADD activity in iDA neurons in vivo. (**A**–**C**) Immunohistochemistry of M3Dq iDA neurons after grafting in *Rag2*$^{-/-}$ *Ilrg*^{tmWjl}–null mice for mCherry and GFP. Scale bar: 30 μm. (**D**) Left: Representative cell-attached recording showing the response of an M3Dq iDA neuron to bath application of CNO (10 μM). The frequency of spontaneous firing was increased after CNO perfusion (control 0.7 ± 0.3 Hz, CNO 5.1 ± 2.4 Hz, washout 0.7 ± 0.5 Hz). Right: Histogram shows the mean firing rate values (± SEM) recorded for 3 to 4 minutes before (Ctrl), during (+ CNO), and after (Washout) CNO application. *P < 0.05 by paired-sample Wilcoxon signed-rank test. (**E**) Representative traces and quantification of evoked dopamine release obtained through FSCV of transplanted M3Dq iDA neurons with and without CNO administration. Data in the right panel represent the means ± SEM. **P < 0.005 by Student's t test. Data shown in **A**–**E** are representative of 3 independent experiments performed on 3 (**A**–**C**), 6 (**D**), or 8 (**E**) samples.

strongly increasing their rate of firing, which persisted for several minutes after the initial challenge (Figure 6A). In contrast, M4Di-expressing iDA neurons silenced their activity for an extended period as soon as they were exposed to CNO (Figure 6B). DREADD receptor signaling is therefore highly effective in modulating neuronal activity in both native and reprogrammed DA neurons. Strikingly, we found that iDA neurons and native DA neurons showed responses to CNO closely resembling the amplitude and timing of neuronal activity.

Sustained neuronal activity is sufficient to increase dopamine production in native DA neurons (43). Thus, we wondered whether M3Dq-expressing iDA neurons respond in a comparable way by raising dopamine levels after sustained neuronal firing triggered by CNO stimulation. To address this question, we stimulated 14-DIV M3Dq iDA neurons by CNO (10 μM) added to fresh culture medium for 10 minutes, harvesting them soon after, followed by lysis and HPLC analysis of their intracellular dopamine content. Of interest, dopamine levels were 3-fold higher after stimulation with CNO, indicating that iDA neurons can respond to increased neuronal activity by enhancing the intracellular synthesis of dopamine (Figure 6D). By contrast, we could not detect a significant variation in dopamine production after CNO stimulation of M4Di-expressing iDA neurons (data not shown). This result is likely because of the low kinetics in reducing dopamine synthesis, making the detection of a significant decrease in neurotransmitter content more challenging. For this reason, we performed the subsequent functional analysis exclusively in M3Dq-expressing iDA neurons.

Next, we asked whether the CNO stimulation of neuronal activity was retained after long-term transplantation of M3Dq-expressing neurons in vivo. To this aim, FACS-sorted TH-GFP^{+} cells expressing the M3Dq-DREADD receptor were transplanted into the striatum of immunodeficient *Rag2*$^{-/-}$ *Ilrg*^{tmWjl}–null mice. We treated the grafted animals with dox for 6 additional days, which was subsequently discontinued until the final time point of analysis was reached 5 weeks after grafting. At this stage, TH-GFP-mCherry double-positive iDA neurons were easily identified in the transplanted sites and exhibited a well-matured neuronal morphology with long fibers spreading in the host brain parenchyma (Figure 7, A–C). We then patch clamped grafted M3Dq-expressing iDA neurons for electrophysiological recordings. Of note, iDA neurons generated fast bursts of APs that continued for several minutes upon CNO acute stimulation (n = 6) (Figure 7D). FSCV measurements of transplanted brain slices also confirmed a significant increase in evoked dopamine release upon CNO treatment (Figure 7E). Altogether, these data confirmed that M3Dq-expressing iDA neurons retain the ability to specifically respond to CNO after integration into the host brain tissue with an increase in electrical activity and dopamine production and release.

iDA neuron engraftments elicit behavioral rescue of 6-OHDA–lesioned rats. Considering the evidence of functional integration of iDA neurons into the host neuronal circuits, we wondered whether the grafted cells could elicit a rescue in 6-OHDA–treated rats and whether this rescue is tunable by the CNO-DREADD system. Rats were subjected to unilateral 6-OHDA injections, and only those displaying a consistent rotational behavior (>6 rotations/minute) were selected for subsequent transplantations. DIV 6–induced M3Dq-expressing TH-GFP^{+} iDA cells were engrafted into 2 independent sites of the lesioned striatum of 6-OHDA–treated rats (n = 10) for a total number of 5 × 10^{5} cells (Figure 8A). In addition, lesioned rats in a second group (n = 10) were engrafted with a similar number of ventral mesencephalon E13.5 DA neurons for direct comparative purposes. Finally, lesioned animals in a third group

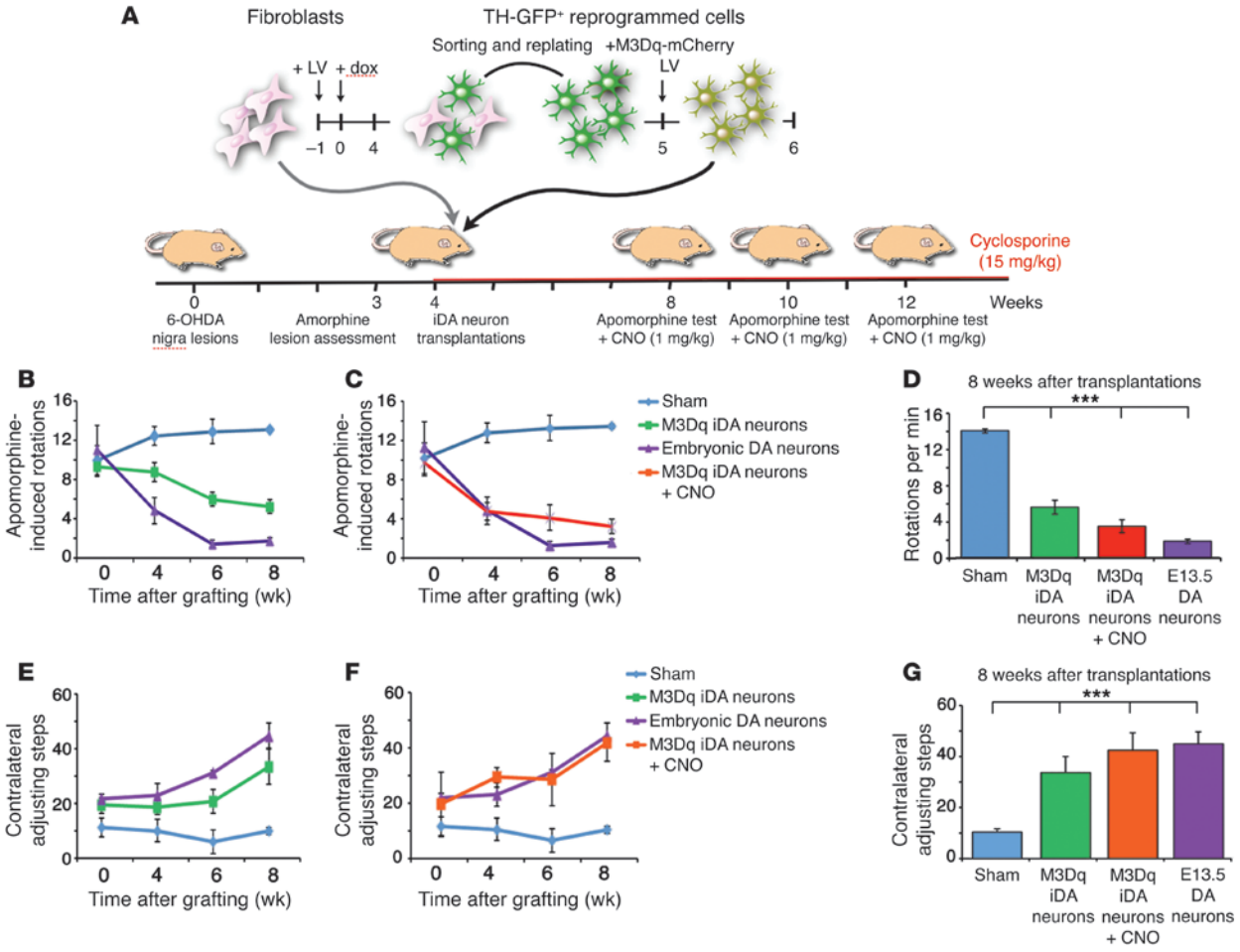

Figure 8

Motor deficit assessment upon CNO administration to parkinsonian rats transplanted with iDA neurons. (**A**) Summary of the experimental procedures for behavioral assays. Selected animals underwent transplantation of M3Dq iDA neurons, control fibroblasts (Sham), and primary embryonic midbrain cells from TH-GFP mice (Embryonic DA neurons). (**B**–**D**) M3Dq iDA neurons and embryonic DA neurons promoted a significant reduction in apomorphine-induced rotation scores that became more evident 8 weeks after grafting. Sham animals showed no recovery of the parkinsonian phenotype. (**C**) CNO administration to animals produced a further amelioration that brought the animals' performance closer to that of animals that received primary DA neurons. (**D**) The number of rotations per minute 8 weeks after transplantation is given as the means ± SEM (n = 10). ***P < 0.001 versus the indicated groups; 1-way ANOVA followed by Bonferroni's multiple comparison test. (**E**–**G**) Recovery of motor impairment was also recorded in the stepping test that was performed with the same timing as that used for the apomorphine-induced rotations. Animals with reprogrammed cells were able to sustain an improvement in the use of the contralateral forelimb that was significant 8 weeks after transplantation (**E**). Also in this behavioral test, CNO administration to grafted animals promoted an enhancement of performance (**F**). (**G**) The number of adjusting steps 8 weeks after transplantation is given as the means ± SEM (n = 10). ***P < 0.001 versus sham; 1-way ANOVA followed by Bonferroni's multiple comparisons test. Data shown in **B**–**G** are representative of 2 independent experiments performed on at least 8 mice per group.

were transplanted with a similar number of TH-GFP fibroblasts, serving as transplanted sham controls (n = 8). We treated all animals with dox for 6 days after cell grafting and kept them under cyclosporine-mediated immunosuppression for the entire duration of the experiment. We tested the graft-induced behavioral recovery in the 3 groups of animals by counting the number of rotations after an acute challenge with apomorphine (0.1 mg/kg) for 60 minutes administered 4, 6, and 8 weeks after transplantation. Although transplanted sham controls did not exhibit any evident alteration in motor performance (blue in Figure 8, B and D), animals with TH-GFP$^+$ iDA neurons showed a significant recovery over time from apomorphine-induced behavior (green in Figure 8, B and D). However, the implanted embryonic DA neurons led to an even more pronounced rescue of the rotational response (violet in Figure 8, B and D). Thus, we found that grafted iDA neurons induced a significant reduction in the asymmetric behavior evoked by apomorphine in lesioned animals, but with less efficiency relative to native primary DA neurons in a side-by-side comparison. An insufficient number of surviving iDA neurons could not be identified as the main cause of the difference, because the numbers of surviving cells were of the same order of magnitude for both reprogrammed and native DA neurons by stereological counting ($3.5 \pm 6 \times 10^4$ and $6.5 \pm 6 \times 10^4$, n = 4, respectively). In percentage terms, the rate of surviving cells obtained from dissection of fetal

tissue was 13%, whereas the survival of iDA neurons was 7%. These quantifications are both in agreement with previous data reported in the literature (18, 32, 44).

We then asked whether the CNO-DREADD system could be directly exploited in vivo, with the aim of further enhancing motor recovery dependent on the transplanted iDA neurons. This approach relies on the known ability of CNO to easily cross the blood-brain barrier when peripherally injected (42). Rats grafted with M3Dq-expressing iDA neurons or fibroblasts were subjected to 1 daily injection of CNO for 3 days (1 mg/kg) before testing of drug-induced turning behavior. Although we found that transplanted sham controls did not show any benefit from this treatment, M3Dq iDA–grafted animals treated with CNO exhibited an enhanced reduction in drug-induced rotational scores that became very closely comparable to those achieved by primary embryonic DA neurons (red in Figure 8, C and D).

As a second functional outcome of cell grafting, we used the stepping test, which measures forelimb akinesia and does not depend on pharmacological stimulation of the DA system. In this case, we obtained a similar pattern of improvements (Figure 8, E and G). Strikingly, in this test, we observed that an increased motor recovery of the iDA neuron–transplanted animals matched the response displayed by animals grafted with primary embryonic DA neurons (Figure 8, F and G). In summary, these results demonstrate the feasibility of the cell reprogramming technology to achieve an outcome comparable to that provided by primary DA neurons and highlight the advantage of DREADDs in specifically stimulating neuronal activity in transplanted neurons and boosting their therapeutic effects in a controllable fashion.

Discussion

This study is the first to our knowledge to focus on the properties of grafted reprogrammed neurons and their ability to integrate into transplanted neural tissue and exert a sustained and persistent behavioral recovery in diseased animals. Most importantly, this functional integration was achieved independently of transgene expression once the reprogrammed state was stably acquired.

Seminal studies have reported that cell replacement–mediated behavioral recovery in animal models of PD is achieved exclusively when DA neurons with a midbrain origin are transplanted into the striatum (44, 45). Midbrain DA neurons are molecularly distinct, in particular for expression of the lineage-specific *Pitx3*, *Foxa1/2*, and *En1/2* genes. Nevertheless, iDA neurons did not express *Pitx3* and *Foxa2* at comparable levels; rather, they displayed a robust expression of *Foxa1*, *En1*, and *En2*. Therefore, ANL-dependent reprogramming enables the acquisition of some of the cardinal molecular features of midbrain-regionalized DA neurons. Thus, it was relevant to ask whether iDA neurons can stably integrate into and functionally mature in the host striatal tissue and alleviate parkinsonian motor deficits.

In this study, we generated evidence that neuronal conversion can be fully reverted if transgene expression is not maintained for a sufficient amount of time. In fact, we showed that TH-GFP$^+$ cells exposed to only 6 days of dox treatment reverted back to fibroblasts in morphology and to collagen expression after brain transplantation. Longer exposure to dox, however, yielded a stable fulfillment of the reprogrammed neuronal state and its phenotypic and functional features. In particular, the iDA neurons stably retained electrical excitability, synaptic currents, and dopamine release after long-term transplantation in healthy as well as in lesioned neural tissues. Here, we provide what we believe to be the first proof that reprogrammed neurons might successfully connect with host neuronal circuits in a functional synaptic network long after transplantation and dox treatment.

With this stable activity and functional integration, transplanted iDA neurons led to a substantial amelioration of drug-induced motor asymmetry in PD rats. Of note, significant recovery was also achieved in the stepping test, which is a drug-independent behavioral assay, and in a stringent read-out of the physiological levels of endogenous dopamine (46). In a side-by-side comparison, however, the grafted iDA neurons resulted in a less effective recovery than was observed in native embryonic DA neurons. In particular, the initial motor asymmetry recovery was slower with induced versus native DA neurons. This outcome likely does not correlate with differences in cell survival after transplantation, because stereological counting showed a comparable number of surviving neurons. The same magnitude of behavioral recovery was obtained when dox was administered for the entire duration of the experiment in a separate group of iDA neuron–transplanted rats (n = 4; data not shown). These findings are consistent with previous results obtained by Kim et al. (32). Therefore, we need to take into consideration the possibility that iDA neurons are intrinsically less functional after in vivo transplantation than their native counterparts.

We favor a different, but not necessarily alternative, explanation, however. The use of 4 separate viruses to express the 3 reprogramming genes and the tetracycline-controlled transactivator (tTA) in the fibroblast cultures inevitably leads to a large heterogeneity at the single-cell level regarding the integration of the transgenes and their consequent expression levels. This extreme variability in transgene expression undoubtedly has a major impact on the correct acquirement of the biochemical and functional neuronal traits in the converted fibroblasts. Even though our experiments were all performed using a FACS-sorted purified TH-GFP$^+$ neuronal population selecting for a homogeneous source of reprogrammed neurons, their relative functional performance could not be anticipated. Consistent with this hypothesis, in our electrophysiological recordings of in vitro cultures, we noted some variability in the functional activity among TH-GFP$^+$ reprogrammed neurons (data not shown). This issue will properly be resolved in the near future by engineering multicistronic vectors for transgene delivery that will ensure homogeneous gene expression levels with proper TF stoichiometry. Similarly, this aspect is absolutely critical for generating high-quality iPS cells after fibroblast reprogramming (47, 48).

To confirm the functional integration of grafted iDA neurons into the host parenchyma, we combined iDA neuronal reprogramming with DREADD technology. This system is powerful for pharmacological manipulation of the neuronal activity and has been applied so far to control the activity of brain neurons in transgenic mice or virally infected cells (42). Significantly, we showed here that this approach is also suitable for controlling the behavior of transplanted neurons. In fact, it provided a mean for the remote control of grafted neuronal activity over time, thereby emphasizing the impact of these neurons on host neuronal circuits. Therefore, this approach can be further exploited to control the disease-modifying activity of transplanted iDA neurons, and our findings validate this technology for pharmacological control of their firing activity. This concept is a fascinating one in PD therapeutics, in which stringent control of dopamine release in the denervated neural targets can exert highly beneficial effects on the pathological symptoms.

DREADD technology is particularly attractive in translational research, because its effects are modulated by CNO, an orally bioavailable drug that is pharmacologically inert with other receptors and easily penetrates the blood-brain barrier (38). Thus, CNO retains a high profile of safety and efficacy that is compatible with its exploitation as a medical treatment. Notwithstanding, for future potential biomedical applications, it has to be taken into account that CNO catabolism implicates the generation of a small amount of clozapine, a drug known to exert some side effects (49).

The present study relies on the powerful neuronal conversion effect triggered by the forced expression of the ANL factor combination on mouse somatic cells. However, the same set of factors is less proficient in reprogramming human cells (30). Additional dopamine fate determinants are beneficial for increasing DA conversion of human fibroblasts (33); however, using a greater number of factors inevitably leads to a more heterogeneously induced neuronal population, hampering the subsequent in vivo functional analysis. Eventually, the development of more amenable genetic elements or improved epigenetic conditions might be more convenient for these functional analyses. Thus, functional studies of human iDA neurons similar to the study presented here will have to wait for further improvement of the methodology for genetic conversion.

In conclusion, this work provides proof that direct cell reprogramming offers a method for obtaining stable and transplantable DA neurons suitable for cell replacement in a PD animal model. Moreover, we show that DREADD technology can be efficiently applied to control the output of reprogrammed neurons. This combination will be of extreme interest for DA cell replacement research and could pave the way for pharmacological approaches aimed at exerting efficient and noninvasive control of the grafted neuronal implant.

Methods

Animals. Mice and rats were maintained in the San Raffaele Scientific Institute's animal facility. All animals were housed on a 12-hour light/12-hour dark cycle with ad libitum access to food and water. Adult male CD rats (200–250 g) and *Rag2*$^{-/-}$ *Ilrg*^{tmWjl} double-KO mice (20–22 g) were used as graft recipients in these experiments, and TH-GFP mice were used for the preparation of MEFs. 6-OHDA–lesioned rats were purchased from Charles River Laboratories and used as a PD model for behavioral tests and histological analysis. Unilateral lesions of the substantia nigra in rats were established by stereotaxic injection of 12 μg of 6-OHDA (3.6 mg/ml, in 0.2% ascorbic acid and 0.9% saline; Sigma-Aldrich) with the following stereotaxic coordinates: AP, –1.5; ML, –1.8; DV, –8.5. The injection side was determined using *The Rat Brain in Stereotaxic Coordinates* atlas by Paxinos and Watson (50). Breeding pairs of TH-GFP mice (51) were provided by S. Gustincich (SISSA, Trieste, Italy), and *Rag2*$^{-/-}$ *Ilrg*^{tmWjl} double-KO mice were provided by P. Ghia (San Raffaele Scientific Institute).

Mouse iDA neuronal cultures. Timed pregnant mice (day of vaginal plug was designated as E0.5) were generated by crossing wild-type CD1 females with transgenic TH-GFP males. On E14.5, the embryos were removed from the pregnant mothers, then GFP$^+$ and wild-type littermates were identified and separated under a fluorescence microscope. Head, vertebral column, dorsal root ganglia, and all internal organs of the GFP$^+$ embryos were removed under a stereomicroscope, and the remaining embryonic tissue was first manually dissociated with a sterile pipette and then incubated in 0.25% trypsin (Sigma-Aldrich) for 30 minutes. Cells from each embryo were plated onto a 15-cm tissue culture dish in MEF media (DMEM containing 10% FBS, β-mercaptoethanol, nonessential amino acids, sodium pyruvate, and penicillin-streptomycin [all from Sigma-Aldrich]). In all experiments, cells were split no more than two times. For cell transplantation procedures, 1.5×10^6 MEFs were plated onto matrigel-coated 10-cm Petri dishes in MEF media. The MEFs were infected with *Ascl1*, *Nurr1*, *Lmx1a*, and tTA lentiviral vectors the following day. Viral vectors were prepared as described elsewhere (30). Sixteen to 20 hours after infection, cells were subjected to neuronal induction through exposure to dox (2 mg/ml; Sigma-Aldrich) resuspended in MEF medium. Two days after induction, the medium was replaced with neuron-inducing medium (DMEM-F12, 25 μg/ml insulin, 50 μg/ml transferrin, 30 nM sodium selenite, 20 nM progesterone, 100 nM putrescine, and penicillin-streptomycin [all from Sigma-Aldrich]) containing dox. Four days after neuronal induction, cells were sorted for GFP and plated onto matrigel-coated 24-well plates at high density (750,000 cells/well) in neuron-inducing medium supplemented with B27 25X and GDNF (Invitrogen). Where appropriate, 24 hours after plating, sorted cells were infected with tdTomato lentiviral vector or M3Dq-IRES-mCherry lentiviral vector (gift of B. Roth, University of North Carolina, Chapel Hill, North Carolina, USA) or with WGA-IRES-mCherry lentiviral vector (gift of A. Basbaum, UCSF, La Jolla, California, USA) in neuron-inducing medium. One day later, cells were harvested in Krebs solution (see below) for transplantation in rats or in immunodepressed mice.

Primary cell cultures. Ventral mesencephalic primary cell cultures were prepared from E13.5 TH-GFP mouse embryos. The ventral mesencephalon was dissected out of each embryo as described previously (52, 53), taking care to remove the meninges. Pooled ventral mesencephala were incubated for 20 minutes at 37°C in HBSS without Ca^{2+} and Mg^{2+} (Euroclone) with 0.1% trypsin and 0.05% DNase. Tissue was mechanically dissociated in HBSS without Ca^{2+} and Mg^{2+} supplemented with 0.05% DNase. Single cells were resuspended in neurobasal medium (Invitrogen) enriched with 30% glucose (Sigma-Aldrich), penicillin-streptomycin (Sigma-Aldrich), L-glutamine (Sigma-Aldrich), and B27 50X (Invitrogen) and seeded onto poly-D-lysine–coated (Sigma-Aldrich) coverslips for electrophysiological experiments at a density of 2.0×10^5 cells/cm^2. For transplantation into parkinsonian rats, 5.0×10^5 cells were resuspended in Krebs solution and injected into 2 sites of the lesioned striatum. For coculture experiments, ventral telencephalon primary cultures were prepared from E14.5 wild-type CD1 embryos, while hippocampal neurons were prepared from E19 rat embryos. The ventral telencephalic structures and hippocampi were dissected out from the forebrain; cell disaggregation and resuspension procedures were previously described for mesencephalic cultures, except for the absence of DNase treatment. A single-cell suspension was seeded onto poly-L-lysine–treated (Sigma-Aldrich) coverslips at a density of 2.5×10^5 cells/cm^2 for ventral telencephalic neurons and at a density of 1×10^5 cells/cm^2 for hippocampal cultures.

RNA isolation and real-time RT-PCR. RNA was extracted using the TRI Reagent isolation system (Sigma-Aldrich) according to the manufacturer's instructions. The yield and integrity of the RNA were determined by the spectrophotometric measurement of A260 and by agarose gel electrophoresis, respectively. Total RNA was treated with DNAse I (Roche) to prevent DNA contamination. One microgram of RNA was reverse transcribed using the Transcriptor High Fidelity cDNA Synthesis Kit (Roche). quantitative RT-PCR (qRT-PCR) was carried out using the CFX96 Real-Time PCR Detection System (Bio-Rad). One-fiftieth of the reverse-transcribed cDNA was amplified in a 25-μl reaction mixture containing 1× SsoFast EvaGreen Supermix (Bio-Rad) and 0.4 mM of each primer. The thermal profile consisted of 2 minutes at 50°C and 10 minutes at 95°C, followed by 40 cycles of 15 seconds each at 95°C and 1 minute at 60°C. mRNA levels were calculated according to the threshold cycle numbers within a linear range of amplification of 20 to 32 cycles. Data were standardized versus the housekeeping gene *Gapdh*, which was used as an internal standard and amplified for every sample in

parallel assays. A melting curve was obtained for each PCR product after each run to confirm that the EvaGreen signal corresponded to a unique and specific amplified product. The primers used for amplification reactions are listed in Supplemental Table 1.

Dopamine determination by HPLC. Cell samples from mouse iDA neurons were lysed in 100 μl of 0.1 M perchloric acid. Samples were sonicated and spun in a microcentrifuge at 10,000 *g* for 10 minutes. The supernatant was transferred in ultra-free microcentrifuge tubes (Millipore, catalog UFC30GV0S) and spun for 10 minutes. Samples (11 μl) were injected into the HPLC apparatus. Measurements of dopamine and metabolites were made by HPLC with an electrochemical detection system (ALEXYS LC-EC; Antec Leyden BV) equipped with a reverse-phase column (3-μm particles, ALB-215 C18, 1 × 150 mm; Antec Leyden BV) at a flow rate of 200 μl/min and electrochemically detected by a 0.7-mm glass carbon electrode (VT-03; Antec Leyden BV). The mobile phase contained 50 mM H_3PO_4, 50 mM citric acid, 8 mM KCl, 0.1 mM EDTA, 400 mg/l octanesulfonic acid sodium salt, and 10% (vol/vol) methanol (pH 3.9).The sensitivity of the method permitted detection of 3 fmol of dopamine.

Electrophysiology on cultured neurons. Recordings were performed from iDA neurons and primary DA neurons 14 days after infection with M3Dq or M4Di lentiviral vectors. APs were recorded in the current-clamp whole-cell configuration. Cells were perfused continuously with HBS with the following composition: 140 mM NaCl, 5 mM KCl, 2 mM $CaCl_2$, 2 mM $MgCl_2$, 15 mM HEPES, and 25 mM glucose (pH 7.4). Patch pipettes with 3 to 5 MΩ resistance were filled with solution containing: 130 mM K-gluconate, 10 mM KCl, 0.5 mM $CaCl_2$, 15 mM HEPES, 5 mM EGTA, 8 mM NaCl, 2 mM MgATP, 0.3 mM Na_2GTP, and 10 mM glucose (pH adjusted to 7.2 with KOH). Vehicle or 10 μM CNO was bath applied through perfusion after achieving a stable baseline for 5 minutes. Recordings were performed using an EPC10 USB patch-clamp amplifier and PATCHMASTER software (HEKA Elektronik). Data were digitized at 10 kHz and analyzed with FITMASTER Software (HEKA Elektronik).

Electrophysiology on brain slices. *Rag2*$^{-/-}$ *Ilrg*^{tmWjl} double-KO mice of either sex (P21–P24) were anesthetized with an intraperitoneal injection of a mixture of ketamine-xylazine (100 mg/kg and 10 mg/kg, respectively) and decapitated. Coronal slices (300-μm-thick) were cut using a Microm HM 650V microtome equipped with a Microm CU 65 cooling unit (Thermo Fisher Scientific) at 2°C in a solution containing 87 mM NaCl, 25 mM $NaHCO_3$, 2.5 mM KCl, 0.5 mM $CaCl_2$, 7 mM $MgCl_2$, 25 mM glucose, 75 mM sucrose and saturated with 95% O_2 and 5% CO_2. After cutting, the slices were left to recover for 30 to 45 minutes at 35°C and for 1 hour at room temperature (RT) in recording solution (see below). Whole-cell and cell-attached patch-clamp recordings were performed with a Multiclamp 700B-Digidata 1440A system (Molecular Devices) on visually identified cells using an upright Olympus BX51WI microscope (Olympus) equipped with a Lambda LS lamp (Sutter). The extracellular solution used for recordings contained: 125 mM NaCl, 25 mM $NaHCO_3$, 2.5 mM KCl, 1.25 mM NaH_2PO_4, 2 mM $CaCl_2$, 1 mM $MgCl_2$, and 25 mM glucose (bubbled with 95% O_2 and 5% CO_2). For voltage- and current-clamp experiments the internal solution contained: 126 mM K-gluconate, 4 mM NaCl, 1 mM $MgSO_4$, 0.02 mM $CaCl_2$, 0.1 mM BAPTA, 15 mM glucose, 5 mM HEPES, 3 mM ATP, and 0.1 mM GTP (pH 7.3). Spontaneous excitatory and inhibitory postsynaptic currents (sEPSCs and sIPSCs) were recorded at a holding potential (V_h) of –70 mV and 0 mV, respectively. Data were acquired at a sampling frequency of 10 kHz, filtered at 2 kHz using pClamp10 software (Molecular Devices) and analyzed with Origin 8.5 (Origin Lab).

Cell transplantation. 6-OHDA lesioned rats were selected for cell transplantation if their apomorphine-induced rotation exceeded 6 rotations per minute 3 weeks after the lesion. Rats were anesthetized with ketamine (90 mg/kg) and xylazine (4 mg/kg) during all surgical procedures. Cells were resuspended in Krebs solution (126 mM NaCl, 2.5 mM KCl, 1.2 mM NaH_2PO_4, 1.2 mM $MgCl_2$, 2.1 mM $CaCl_2$, 11 mM glucose, and 25 mM $NaHCO_3$) and transplanted into 2 sites of the lesioned striatum of each animal (coordinates: AP, +1.5, +0.7; ML, +3.0; DV, –5.0) using a 5-μl Hamilton syringe. For each injection site, 4 μl of cell suspension was injected at a flow rate of 1 μl/minute. A total of 5×10^5 cells were injected into each rat. The needle was left in place for 2 minutes after each injection. Control rats (sham) received fibroblasts instead. A daily intraperitoneal injection of 15 mg/kg cyclosporine (Sandimmune, 50 mg/ml; Novartis) was started 24 hours before cell grafting and continued until death.

Rag2$^{-/-}$ *Ilrg*^{tmWjl} double-KO mice were anesthetized with avertin and transplanted with 4×10^5 cells resuspended in Krebs solution in a volume of 4 μl. Cells were grafted into the striatum at the following coordinates: AP, +0.5; ML, +1.8; DV, –3.2.

Behavioral assays. Apomorphine-induced rotations and stepping tests in lesioned rats were carried out before transplantation and 4, 6, and 8 weeks after transplantation. Rotational behavior was recorded for 60 minutes after intraperitoneal injection of 0.1 mg/kg apomorphine (Sigma-Aldrich) and automatically assessed using a rotameter (Panlab). Data were presented as the average number of rotations per minute. The stepping test was performed as described previously (18). Briefly, during the procedure, the rat was held by the experimenter, who fixed the hind limbs with one hand and alternatively the left or the right forelimb with the other hand. In this way, the animal was allowed to touch the table surface with only one forelimb at a time. The rat was then pulled over a 1-meter surface, first in the forehand and then in the backhand direction. This test relies on the evidence that unilaterally lesioned animals show a clear impairment of motor performance in the paw contralateral to the lesion. Therefore, unilaterally lesioned animals will step on the bench while being moved by the operator with the ipsilateral forelimb. By contrast, the contralateral paw will be passively dragged. On this basis, an amelioration of motor deficits after transplantation can be easily quantified by counting the contralateral steps performed by treated and sham animals over time. This procedure was applied to collect the data shown in Figure 8.

FSCV. Transplanted mice and rats were anesthetized with halothane and then decapitated. The brain was sectioned in cold carboxygenated artificial cerebrospinal fluid (aCSF) (126 mM NaCl, 2.5 mM KCl, 1.2 mM NaH_2PO_4, 25 mM $NaHCO_3$, 2.4 mM $CaCl_2$, 11 mM D-glucose, and 1.2 mM $MgCl_2$) on a VT1000S vibratome (Leica Microsystems) at a thickness of 300 μm. Coronal slices containing the dorsal striatum and nucleus accumbens were allowed to recover for at least 1 hour at RT in carboxygenated aCSF. For recordings, slices were superfused with 32°C carboxygenated aCSF at a flow rate of 1 ml/minute. Experimental recordings started 20 minutes after transfer to the slice chamber. Carbon fiber electrodes (7 μm; Goodfellow) were made as previously described (54, 55). They were trimmed to obtain a basal current between 140 and 180 nA. The electrodes were inserted approximately 100 μm into the dorsal striatal brain slice. The potential of the working electrode was held at –0.4 V versus Ag/AgCl between scans and was ramped to +1.3 V at 300 V/second and back to –0.4 V every 100 ms via an EVA8 amplifier (HEKA Elektronik). Axonal dopamine release in the striatum was evoked using a twisted bipolar stimulating electrode (Plastics One). Stimulations were delivered every 2 minutes by a single electrical pulse (0.1 ms, single stimulus) or with a train of stimuli (20 pulses at 10 Hz). The pulse amplitude was 400 μA for both single and train pulses. The stimulus was delivered via a stimulus isolator (A-M Systems). Background-subtracted cyclic voltammograms were obtained by subtracting the current obtained before the stimulation from all recordings. The peak oxidation current for dopamine in each voltammogram was converted into a measurement of the dopamine concentration by postcalibration of the electrode using 1 μM dopamine (Sigma-Aldrich).

Data were normalized to the first 5 recordings (10 minutes) of the respective control period and plotted versus time (means ± SEM). TarHeel CV (ESA Biosciences) was used for all data analysis.

Tissue processing. Mice and rats received overdoses of pentobarbital (50 mg/kg) intraperitoneally to induce deep anesthesia. All animals were transcardially perfused with 0.9% saline, followed by ice-cold PFA (4% w/v in PBS; Sigma-Aldrich). Brains were removed, postfixed overnight in 4% PFA, and cryoprotected in 30% sucrose (Sigma-Aldrich) for 2 to 5 days before being sectioned on a Leica cryostat. Coronal sections were collected in 12 series for rats and 6 series for mice at a thickness of 40 μm.

Immunohistochemistry. Free-floating sections were collected in PBS and washed 3 times in PBS between each step in the immunohistochemical protocol. For detection of the antigens with fluorescent antibodies, the protocol was performed as follows: sections were left in blocking solution (PBS supplemented with 1% goat serum and 0.1% Triton) for 1 hour at RT and then incubated overnight at 4°C with primary antibodies diluted in blocking solution. The following day, sections were incubated for 2 hours at RT with appropriate Alexa 488 or Alexa 594 secondary antibodies supplemented with Hoechst (Invitrogen) for nuclear staining. The free-floating sections were finally mounted on slides before being coverslipped with fluorescence mounting medium (Dako).

For peroxidase-based reactions, endogenous peroxidase activity was quenched for 15 minutes with 3% H_2O_2 before application of blocking solution. Primary antibodies were applied as previously described. Biotinylated secondary antibodies were applied for 1 hour at RT, followed by incubation with the streptavidin-horseradish peroxidase complex (ABC Elite kit, Vectastain; Vector Laboratories) for 1 hour. Sections were then exposed to 0.5 mg/ml diamino-benzidine (Sigma-Aldrich), and precipitation of the chromophore was catalyzed by the addition of 1% H_2O_2, followed by final washing with PBS. Sections were mounted on slides as mentioned above.

The following primary antibodies and dilution factors were used: mouse anti-tyrosine hydroxylase (1:200; Millipore), rabbit anti-tyrosine hydroxylase (1:200; Immunological Sciences), chicken anti-GFP (1:1,000; Molecular Probes), rabbit anti-VMAT2 (1:200; Immunological Sciences), rabbit anti-WGA (1:2,000; Sigma-Aldrich), rabbit anti-Homer1 (1:100; Synaptic Systems), mouse anti-SYT1 (1:100; Synaptic Systems), rabbit anti-DsRed (1:500; Clontech), rabbit anti-AADC (1:100; Novus), rat anti-DAT (1:100; Chemicon), and rabbit anti-Ki67 (1:500; Immunological Sciences). For detection of functional VMAT2 on iDA neurons, the FFN511 probe was used as previously described (40). For immunodetection of biocytin-filled neurons, Alexa Fluor 546–conjugated streptavidin (Invitrogen) was used at a dilution factor of 1:500.

Cell counting and stereological analysis. Cells were quantified with the assistance of Stereo Investigator software, version 3.0 (MicroBrightField) and a personal computer connected to a color video camera mounted on a Leica microscope (56, 57). The motorized stage of the microscope allowed precise and well-defined movements along the *x*-, *y*-, and *z* axes. Images were first acquired with a CCD-IRIS color video camera, and the cerebral hemispheres were interactively delineated at low magnification on a video image of the section. The number of iDA neurons contained in each graft was estimated through extrapolation of the total number of GFP^+ cells detected by DAB immunohistochemistry that were counted in every third tissue section at ×40 magnification. To estimate the total number of GFP^+ cells, the number of neurons counted on the sections was multiplied by 3.

Statistics. Data were analyzed using the 2-tailed Student's *t* test or, in cases of more than 2 experimental groups, by 1- or 2-way ANOVA followed by the post-hoc Bonferroni's multiple comparison test. Non-normally distributed data were analyzed by the corresponding nonparametric tests. Statistical analysis was carried out using Sigmaplot 12.0 software (Systat Software). Statistical significance was set at $P < 0.05$. Data are expressed throughout as the means ± SEM.

Study approval. All mouse experiments were conducted in accordance with the guidelines established by the European Communities Council (Directive 2010/63/EU of September 22, 2010) and were approved by the local IACUC of the San Raffaele Scientific Institute (Milan, Italy).

Acknowledgments

We thank B. Roth, M. Iannacone, S. Curreli, P. Ghia, and J.M. Braz for helpful discussion and for sharing their reagents. This study was supported by grants from the Italian Ministry of Health; the European Research Council (ERC); the Fondazione Grigioni per il Morbo di Parkinson; the IIT-SEED project; Eranet Neuron; the Cariplo Foundation and the Michael J. Fox Foundation (to V. Broccoli); Telethon-GGP11095 (to V. Broccoli and A. Dityatev); Telethon-GGP13033 (to F. Benfenati); the EC FP7-HEALTH-2013-INNOVATION integrating project "Desire" (to F. Benfenati, S. Taverna, and V. Broccoli); the Fondazione Istituto Italiano di Tecnologia (to S. Taverna, R.R. Gainetdinov, A. Dityatev, and F. Benfenati); and EU/FP7 ICT-FET (to S. Taverna).

Received for publication December 10, 2013, and accepted in revised form April 24, 2014.

Address correspondence to: Vania Broccoli, Stem Cells and Neurogenesis Unit, Division of Neuroscience, San Raffaele Scientific Institute, Via Olgettina 58, 20132 Milan, Italy. Phone: 39.02.26434616; Fax: 39.02.26434621; E-mail: broccoli.vania@hsr.it.

1. Cherry AB, Daley GQ. Reprogramming cellular identity for regenerative medicine. *Cell*. 2012; 148(6):1110–1122.
2. Graf T, Enver T. Forcing cells to change lineages. *Nature*. 2009;462(7273):587–594.
3. Holmberg J, Perlmann T. Maintaining differentiated cellular identity. *Nat Rev Genet*. 2012;13(6):429–439.
4. Takahashi K, Yamanaka S. Induction of pluripotent stem cells from mouse embryonic and adult fibroblasts cultures by defined factors. *Cell*. 2006; 126(4):663–676.
5. Takahashi K, et al. Induction of pluripotent stem cells from adult human fibroblasts by defined factors. *Cell*. 2007;131(5):861–872.
6. Espuny-Camacho I, et al. Pyramidal neurons derived from human pluripotent stem cells integrate efficiently into mouse brain circuits in vivo. *Neuron*. 2013;77(3):440–456.
7. Hansen DV, Rubenstein JL, Kriegstein AR. Deriving excitatory neurons of the neocortex from pluripotent stem cells. *Neuron*. 2011;70(4):645–660.
8. Koch P, Kokaia Z, Lindvall O, Brüstle O. Emerging concepts in neural stem cell research: autologous repair and cell-based disease modelling. *Lancet Neurol*. 2009;8(9):819–829.
9. Maroof AM, et al. Directed differentiation and functional maturation of cortical interneurons from human embryonic stem cells. *Cell Stem Cell*. 2013; 12(5):559–572.
10. Nicholas CR, et al. Functional maturation of hPSC-derived forebrain interneurons requires an extended timeline and mimics human neural development. *Cell Stem Cell*. 2013;12(5):573–586.
11. Shi Y, Kirwan P, Smith J, Robinson HP, Livesey FJ. Human cerebral cortex development from pluripotent stem cells to functional excitatory synapses. *Nat Neurosci*. 2012;15(3):477–486.
12. Barker RA, Barrett J, Mason SL, Björklund A. Fetal dopaminergic transplantation trials and the future of neural grafting in Parkinson's disease. *Lancet Neurol*. 2013;12(1):84–91.
13. Brundin P, Barker RA, Parmar M. Neural grafting in Parkinson's disease Problems and possibilities. *Prog Brain Res*. 2010;184:265–294.
14. Koch P, Opitz T, Steinbeck JA, Ladewig J, Brüstle O. A rosette-type, self-renewing human ES cell-derived neural stem cell with potential for in vitro instruction and synaptic integration. *Proc Natl Acad Sci U S A*. 2009;106(9):225–230.
15. Hargus G, et al. Differentiated Parkinson patient-derived induced pluripotent stem cells grow in the adult rodent brain and reduce motor asymmetry in Parkinsonian rats. *Proc Natl Acad Sci U S A*. 2010;107(36):15921–15926.
16. Kim JH, et al. Dopamine neurons derived from embryonic stem cells function in an animal model of Parkinson's disease. *Nature*. 2002;418(6893):50–56.
17. Kirkeby A, et al. Generation of regionally specified neural progenitors and functional neurons from human embryonic stem cells under defined conditions. *Cell Rep*. 2012;1(6):703–714.
18. Kriks S, et al. Dopamine neurons derived from human ES cells efficiently engraft in animal

models of Parkinson's disease. *Nature*. 2011; 480(7378):547–551.
19. Roy NS, Cleren C, Singh SK, Yang L, Beal MF, Goldman SA. Functional engraftment of human ES cell-derived dopaminergic neurons enriched by coculture with telomerase-immortalized midbrain astrocytes. *Nat Med*. 2006;12(11):1259–1268.
20. Wernig M, et al. Neurons derived from reprogrammed fibroblasts functionally integrate into the fetal brain and improve symptoms of rats with Parkinson's disease. *Proc Natl Acad Sci U S A*. 2008; 105(15):5856–5861.
21. Ben-David U, Benvenisty N. The tumorigenicity of human embryonic and induced pluripotent stem cells. *Nat Rev Cancer*. 2011;11(4):268–277.
22. Vierbuchen T, Ostermeier A, Pang ZP, Kokubu Y, Südhof TC, Wernig M. Direct conversion of fibroblasts to functional neurons by defined factors. *Nature*. 2010;463(7284):1035–1041.
23. Ambasudhan R, et al. Direct reprogramming of adult human fibroblasts to functional neurons under defined conditions. *Cell Stem Cell*. 2011; 9(2):113–118.
24. Pang ZP, et al. Induction of human neuronal cells by defined transcription factors. *Nature*. 2011; 476(7359):220–223.
25. Pfisterer U, et al. Direct conversion of human fibroblasts to dopaminergic neurons. *Proc Natl Acad Sci U S A*. 2011;108(25):10343–10348.
26. Yoo AS, et al. MicroRNA-mediated conversion of human fibroblasts to neurons. *Nature*. 2011; 476(7359):228–231.
27. Ang SL. Transcriptional control of midbrain dopaminergic neuron development. *Development*. 2006;133(18):3499–3506.
28. Smidt MP, Burbach JP. How to make a mesodiencephalic dopaminergic neuron. *Nat Rev Neurosci*. 2007; 8(1):21–32.
29. Wallén A, Perlmann T. Transcriptional control of dopamine neuron development. *Ann N Y Acad Sci*. 2003;991:48–60.
30. Caiazzo M, et al. Direct generation of functional dopaminergic neurons from mouse and human fibroblasts. *Nature*. 2011;476(7359):224–227.
31. Addis RC, Hsu FC, Wright RL, Dichter MA, Coulter DA, Gearhart JD. Efficient conversion of astrocytes to functional midbrain dopaminergic neurons using a single polycistronic vector. *PLoS One*. 2011; 6(12):e28719.
32. Kim J, et al. Functional integration of dopaminergic neurons directly converted from mouse fibroblasts. *Cell Stem Cell*. 2011;9(5): 413–419.
33. Torper O, et al. Generation of induced neurons via direct conversion in vivo. *Proc Natl Acad Sci U S A*. 2013;110(17):7038–7043.
34. Heinrich C, et al. Directing astroglia from the cerebral cortex into subtype specific functional neurons. *PLoS Biol*. 2010;8(5):e1000373.
35. Son EY, et al. Conversion of mouse and human fibroblasts into functional spinal motor neurons. *Cell Stem Cell*. 2011;9(3):205–218.
36. Yang N, Ng YH, Pang ZP, Südhof TC, Wernig M. Induced neuronal cells: how to make and define a neuron. *Cell Stem Cell*. 2011;9(6):517–525.
37. Alexander GM, et al. Remote control of neuronal activity in transgenic mice expressing evolved G protein-coupled receptors. *Neuron*. 2011;63(1):27–39.
38. Armbruster BN, Li X, Pausch MH, Herlitze S, Roth BL. Evolving the lock to fit the key to create a family of G protein-coupled receptors potently activated by an inert ligand. *Proc Natl Acad Sci U S A*. 2007; 104(12):5163–5168.
39. Rogan SC, Roth BL. Remote control of neuronal signaling. *Pharmacol Rev*. 2011;63(2):291–315.
40. Gubernator NG, et al. Fluorescent false neurotransmitter visualize dopamine release from individual presynaptic terminals. *Science*. 2009; 324(5933):1441–1444.
41. Capotondo A, et al. Brain conditioning is instrumental for successful microglia reconstitution following hematopoietic stem cell transplantation. *Proc Natl Acad Sci U S A*. 2012;109(37):15018–11523.
42. Wess J, Nakajima K, Jain S. Novel designer receptors to probe GPCR signaling and physiology. *Trends Pharmacol Sci*. 2013;34(7):385–392.
43. Sombers LA, Beyene M, Carelli RM, Wightman RM. Synaptic overflow of dopamine in the nucleus accumbens arises from neuronal activity in the ventral tegmental area. *J Neurosci*. 2009;29(6):1735–1742.
44. Thompson L, Bjorklund A. Survival, differentiation and connectivity of ventral mesencephalic dopamine neurons following transplantation. *Prog Brain Res*. 2012;200:61–95.
45. Lindvall O, Björklund A. Cell therapeutics in Parkinson's disease. *Neurotherapeutics*. 2011;8(4):539–848.
46. Olsson M, Nikkhah G, Bentlage C, Björklund A. Forelimb akinesia in the rat Parkinson model: differential effects of dopamine agonists and nigral transplants as assessed by a new stepping test. *J Neurosci*. 1995;15(5 pt 2):3863–3875.
47. Carey BW, et al. Reprogramming factor stoichiometry influences the epigenetic state and biological properties of induced pluripotent stem cells. *Cell Stem Cell*. 2011;9(6):588–598.
48. Stadtfeld M, Maherali N, Borkent M, Hochedlinger K. A reprogrammable mouse strain from gene-targeted embryonic stem cells. *Nat Methods*. 2010; 7(1):53–55.
49. Jann MW, Lam YW, Chang WH. Rapid formation of clozapine in guinea pigs and man following clozapine-N-oxide administration. *Arch Int Pharmacodyn Ther*. 1994;328(2):243–250.
50. Paxinos G, Watson C, eds. *The Rat Brain In Stereotaxic Coordinates*. San Diego, California, USA: Academic Press; 1997.
51. Sawamoto K, et al. Visualization, direct isolation and transplantation of midbrain dopaminergic neurons. *Proc Natl Acad Sci U S A*. 2001; 98(11):6423–6428.
52. Dunnett SB, Bjorklund A. Staging and dissection of rat embryos. In: Dunnet SB, Bjorklund A, eds. *Neural Transplantation, A Practical Approach*. Oxford, United Kingdom: Oxford University Press; 1992:1–18.
53. Dunnett SB, Bjorklund A. Dissecting embryonic neural tissues for transplantation. In: Dunnett SB, Bjorklund A, Barker GB, eds. *Neuromethods: Cell And Tissue Transplantation In The Cns*. Totowa, New Jersey: Humana Press; 2000:3–25.
54. Kawagoe KT, Zimmerman JB, Wightman RM. Principles of voltammetry and microelectrode surface states. *J Neurosci Methods*. 1993;48(3):225–240.
55. Kuhr WG, Wightman RM. Real-time measurement of dopamine release in rat brain. *Brain Res*. 1986; 381(1):168–171.
56. West MJ, Slomianka L, Gundersen H. Unbiased stereological estimation of the total number of neurons in the subdivisions of the rat hippocampus using the optical fractionator. *Anat Rec*. 1991; 231(4):482–497.
57. Bacigaluppi M, Pluchino S, Peruzzotti-Jametti L, et al. Delayed post-ischaemic neuroprotection following systemic neural stem cell transplantation involves multiple mechanisms. *Brain*. 2009; 132(pt 8):2239–2251.